January 2008

A six-dimensional H_2–H_2 potential energy surface for bound state spectroscopy

Robert Hinde
University of Tennessee, rhinde@utk.edu

Follow this and additional works at: http://trace.tennessee.edu/utk_chempubs

Part of the Atomic, Molecular and Optical Physics Commons, Biological and Chemical Physics Commons, and the Physical Chemistry Commons

A six-dimensional H_2-H_2 potential energy surface for bound state spectroscopy

Robert J. Hinde[a)]

Department of Chemistry, University of Tennessee, Knoxville, Tennessee 37996-1600, USA

We present a six-dimensional potential energy surface for the $(H_2)_2$ dimer based on coupled-cluster electronic structure calculations employing large atom-centered Gaussian basis sets and a small set of midbond functions at the dimer's center of mass. The surface is intended to describe accurately the bound and quasibound states of the dimers $(H_2)_2$, $(D_2)_2$, and H_2-D_2 that correlate with H_2 or D_2 monomers in the rovibrational levels $(v,j)=(0,0)$, (0,2), (1,0), and (1,2). We employ a close-coupled approach to compute the energies of these bound and quasibound dimer states using our potential energy surface, and compare the computed energies for infrared and Raman transitions involving these states with experimentally measured transition energies. We use four of the experimentally measured dimer transition energies to make two empirical adjustments to the *ab initio* potential energy surface; the adjusted surface gives computed transition energies for 56 experimentally observed transitions that agree with experiment to within 0.036 cm^{-1}. For 26 of the 56 transitions, the agreement between the computed and measured transition energies is within the quoted experimental uncertainty. Finally, we use our potential energy surface to predict the energies of another 34 not-yet-observed infrared and Raman transitions for the three dimers. © *2008 American Institute of Physics*. [DOI: 10.1063/1.2826340]

I. INTRODUCTION

The $(H_2)_2$ dimer has long been viewed as a prototypical bimolecular van der Waals dimer. Because the $(H_2)_2$ dimer is electronically simple, it has been the focus of a number of *ab initio* studies;[1–16] however, because the H_2-H_2 van der Waals interaction is quite weak,[17] *ab initio* calculations with accuracy much higher than the oft-quoted "chemical accuracy" of 1 kcal/mol must be employed to provide useful information about the H_2-H_2 potential energy surface. Two recent advances in *ab initio* methods have made it possible to compute the H_2-H_2 interaction with the required level of accuracy: (1) The development of hierarchical sequences of one-electron Gaussian basis sets for approximating molecular electronic wave functions,[18] sequences which systematically approach the complete one-electron basis-set limit, and (2) the development of efficient methods for accounting for electron correlation effects in these wave functions by systematically approaching the many-electron basis-set limit.[19,20]

Diep and Johnson[14] took advantage of these two advances in *ab initio* methods to compute an accurate four-dimensional rigid-rotor potential energy surface for the $(H_2)_2$ dimer; the Diep-Johnson surface gives low-temperature second virial coefficients and integral elastic scattering cross sections in reasonably good agreement with experiment. However, this potential energy surface does not depend explicitly on the covalent bond lengths of the two H_2 monomers, and thus is only able to describe the interaction between two H_2 molecules in their $v=0$ vibrational ground states.

More recently, Boothroyd *et al.*[16] have compiled a large database of energies for the H_4 system, based largely on multireference configuration interaction *ab initio* calculations, and have fit a global six-dimensional H_4 potential energy surface to these energies. However, in this database, $(H_2)_2$ dimer configurations representative of the van der Waals well are assigned energies that come not from *ab initio* calculations but rather from an empirically modified rigid-rotor potential energy surface. Recent theoretical studies of low-energy inelastic H_2-H_2 collisions that use this potential energy surface[21–23] yield computed energy transfer rate coefficients in rather poor agreement with experiment.

The $(H_2)_2$ dimer has also been the focus of several experimental investigations, beginning with the pioneering work of Watanabe and Welsh[24] that demonstrated the dimer's existence through observation of its infrared (IR) absorption spectrum in the H_2 $v=1\leftarrow0$ vibrational fundamental band. Later experimental studies[25,26] recorded at high resolution the IR absorption spectra of the $(H_2)_2$ dimer (and several of its isotopomers) in the $v=1\leftarrow0$ fundamental band and $v=2\leftarrow0$ first overtone band of the corresponding monomers. The high-resolution IR absorption spectra of $(H_2)_2$ in the H_2 fundamental and overtone regions, and the analogous isotopomer spectra, provide information about the vibrational dependence of the H_2-H_2 interaction. Complementary studies[27] of the far-IR absorption spectrum of the dimer provide information about the anisotropy of the potential energy surface in the region of the van der Waals well.

Recently, the Raman spectrum of the $(H_2)_2$ dimer in the H_2 fundamental region has also been observed.[28] This spectrum provides information about the vibrational dependence of the H_2-H_2 interaction that is complementary to that pro-

a)Electronic mail: rhinde@utk.edu.

    128, 154308-1

vided by the high-resolution IR studies. Specifically, the vibrationally excited state of $(H_2)_2$ that is probed by the IR studies is one in which the vibrational excitation is delocalized across the two H_2 monomers in an antisymmetric fashion, while in the Raman studies, the excited $(H_2)_2$ state is one in which the vibrational excitation is delocalized symmetrically across the two monomers. A comparison of the IR and Raman spectra thus provides insight into the coupling between the two H_2 vibrational modes in the $(H_2)_2$ complex and into the dependence of the H_2-H_2 potential energy surface on the two monomers' bond lengths.

Equipped with this new information, we attempt here the construction of a six-dimensional H_2-H_2 potential energy surface that accurately describes the dimer's van der Waals well. We begin by computing *ab initio* H_2-H_2 interaction energies that are nearly converged with respect to both the one-electron and many-electron basis sets, and then construct a smooth potential energy surface from these computed interaction energies. We then make two small empirical adjustments to the surface; these adjustments soften slightly the surface's short-range repulsive wall, and increase slightly the strength of the surface's anisotropic term that couples the rotational degrees of freedom of the two monomers. The empirically adjusted surface gives IR and Raman transition energies for the $(para-H_2)_2$, $(ortho-D_2)_2$, and $para-H_2-ortho-D_2$ dimers in good agreement with available experimental data.[25,27,28]

II. *AB INITIO* COMPUTATIONS

A. Functional form of the H_2-H_2 interaction

We consider a space-fixed coordinate system (x, y, z) in which one H_2 molecule (denoted molecule 1) has its center of mass at the origin and the other H_2 molecule (denoted molecule 2) has its center of mass on the positive z axis. The orientation of molecule i is specified by its spherical polar and azimuthal angles (θ_i, ϕ_i). We let R represent the distance between the molecules' centers of mass, and let r_i represent the bond length of molecule i. The H_2-H_2 potential energy surface can then be expanded in terms of coupled spherical harmonics:[29]

$$V = \sum_{l_1, l_2, L} A_{l_1, l_2, L}(R, r_1, r_2) G_{l_1, l_2, L}(\theta_1, \theta_2, \phi), \quad (1)$$

where $\phi = \phi_2 - \phi_1$, the summation indices l_1, l_2, and L are non-negative integers that must satisfy

$$l_1 + l_2 + L = \text{even integer}, \quad (2)$$

and the homonuclear symmetry of the two H_2 monomers dictates that l_1 and l_2 are also both even. The angular functions $G_{l_1, l_2, L}$ have the form

$$G_{l_1, l_2, L} = \sqrt{\frac{2L+1}{4\pi}} \sum_m C(l_1, m, l_2, -m; L, 0)$$
$$\times Y_{l_1, m}(\theta_1, \phi_1) Y_{l_2, -m}(\theta_1, \phi_2), \quad (3)$$

where C is a Clebsch-Gordan coefficient and $Y_{l,m}$ is a spherical harmonic normalized so that $Y_{l,m}(0,0) = \delta_{m,0}\sqrt{(2l+1)/4\pi}$. (We use the Condon-Shortley phase con-

vention for $Y_{l,m}$.) The appearance of the Clebsch-Gordan coefficient C in Eq. (3) means that l_1, l_2, and L must satisfy the angular momentum triangle rule.

The functions $G_{l_1, l_2, L}$ constitute a complete, orthogonal basis set for functions of the three angular coordinates $(\theta_1, \theta_2, \phi)$. For fixed R, r_1, and r_2, the coefficient $A_{l_1, l_2, L}(R, r_1, r_2)$ can therefore be computed as

$$A_{l_1, l_2, L}(R, r_1, r_2)$$
$$= \frac{1}{2L+1} \int \int G_{l_1, l_2, L}(\theta_1, \theta_2, \phi) V(R, r_1, r_2, \theta_1, \theta_2, \phi) dS_1 dS_2, \quad (4)$$

where $dS_i = \sin \theta_i d\theta_i d\phi_i$.

Earlier studies of the four-dimensional rigid-rotor H_2-H_2 potential energy surface[14,17] show that the surface is dominated by four terms, with $(l_1, l_2, L) = (0,0,0)$, $(0,2,2)$, $(2,0,2)$, and $(2,2,4)$. In this work, we use numerical quadrature to compute the right-hand side of Eq. (4) for these four (l_1, l_2, L) triples. Specifically, at fixed values of R, r_1, and r_2, we use the 18-point spherical quadrature rule numbered 25.4.64 in Ref. 30 to evaluate the integrals over both dS_1 and dS_2 in Eq. (4). This requires us to compute the H_2-H_2 interaction energy $V(R, r_1, r_2, \theta_1, \theta_2, \phi)$, using *ab initio* quantum chemical methods that we describe below, at 12 sets of angles $(\theta_1, \theta_2, \phi)$ when $r_1 = r_2$ and at 19 sets of angles when $r_1 \neq r_2$. Symmetry relationships allow the rest of the $18^2 = 324$ interaction energies at fixed (R, r_1, r_2) to be determined from these *ab initio* calculations.

The accuracy of the $A_{l_1, l_2, L}$ coefficients computed in this fashion is limited by the fact that the quadrature rule we use fails to reproduce the orthogonality conditions

$$\int \int G_{l_1, l_2, L}(\theta_1, \theta_2, \phi) G_{l_1', l_2', L'}(\theta_1, \theta_2, \phi) dS_1 dS_2$$
$$= \delta_{l_1, l_1'} \delta_{l_2, l_2'} \delta_{L, L'}(2L+1) \quad (5)$$

when $l_1 + l_1' \geq 6$ or $l_2 + l_2' \geq 6$. This means that the value of $A_{0,0,0}$ obtained via quadrature also includes some contamination from $A_{6,0,6}$ and $A_{0,6,6}$ (if these coefficients are nonzero in the *ab initio* potential energy surface), while $A_{2,2,4}$ is contaminated by (among other terms) $A_{2,4,6}$ and $A_{4,2,6}$, which describe the long-range electrostatic quadrupole–hexadecapole (QH) interaction between the two H_2 molecules.

To assess the magnitude of these erroneous contributions to the four $A_{l_1, l_2, L}$ coefficients of interest, we used the more accurate 24-point spherical quadrature rule of Ref. 30 to calculate the coefficients at $(R, r_1, r_2) = (4.5a_0, 1.4a_0, 1.7a_0)$, a repulsive $(H_2)_2$ configuration where we expect the angular anisotropy of the potential energy surface to be relatively high, and where this contamination should thus be relatively severe. Table I compares the coefficients obtained using the two quadrature rules (based on *ab initio* interaction energies computed using the protocol outlined in Sec. II B); the errors introduced at this (R, r_1, r_2) configuration by using 18-point quadrature appear to be quite small for the four terms that we include in our final potential energy surface. This table also

TABLE I. Comparison of angular expansion coefficients $A_{l_1,l_2,L}$ (in cm^{-1}) computed using two spherical quadrature rules at (R, r_1, r_2) $=(4.5a_0, 1.4a_0, 1.7a_0)$. These coefficients do not include the full-triples correction.

(l_1, l_2, L)	18 point	24 point
(0, 0, 0)	674.559	674.629
(0, 2, 2)	32.984	33.577
(2, 0, 2)	20.195	20.465
(2, 2, 4)	19.017	19.174
(2, 2, 0)	−0.599	1.413
(2, 2, 2)	0.465	−0.292

gives the values for two additional coefficients in the coupled spherical harmonic expansion, $A_{2,2,0}$ and $A_{2,2,2}$, at this $(H_2)_2$ configuration, and shows that they are one to two orders of magnitude smaller than any of the four terms we retain in Eq. (1). This is in accord with previous studies[14,17] of the four-dimensional rigid-rotor H_2-H_2 potential energy surface.

B. CCSD(T) *ab initio* calculations

We use GAUSSIAN 03 (Ref. 31) to compute the H_2-H_2 interaction energy, employing a coupled-cluster[19,20] treatment of electron correlation that includes single and double excitations and a perturbative treatment of triple excitations,[32] abbreviated CCSD(T). The CCSD(T) calculations are based on a restricted Hartree-Fock reference wave function; we have verified that such a reference does not exhibit a restricted → unrestricted instability for the H_2 bond lengths considered here. We use the aug-cc-pVQZ basis set[18,33] for the four hydrogen atoms, supplement this atom-

centered basis set with a set of $(3s3p2d)$ bond functions positioned at the dimer's center of mass, and employ the standard counterpoise correction.[34] The bond function exponents are taken from Ref. 35.

We carry out these calculations at r_1 and r_2 values of 1.1, 1.4, and $1.7a_0$, and at 19 R values ranging from $R=4.25a_0$ to $12.0a_0$, for a total of 1653 unique $(R, r_1, r_2, \theta_1, \theta_2, \phi)$ $(H_2)_2$ configurations. We turn off automatic checking of the one-electron overlap matrix for near linear dependence and retain all 206 one-electron basis functions at every configuration; this eliminates possible discontinuities in the potential energy surface that could arise when some of these functions are dropped from the one-electron basis set. The GAUSSIAN 03 H_2-H_2 total CCSD(T) energies for these configurations are available from the EPAPS depository.[36] We have checked a small subset of these energies against calculations using the DALTON *ab initio* code;[37] the dimer total energies computed using the two codes agree to within 2×10^{-8} hartree or better.

To assess the error introduced by truncating the one-electron basis set at the aug-cc-pVQZ+$(3s3p2d)$ level, we performed some calculations at selected configurations using a smaller aug-cc-pVTZ atom-centered basis set and the same $(3s3p2d)$ bond function set. The coefficients $A_{l_1,l_2,L}$ obtained from these two sets of *ab initio* interaction energies are listed in Table II. The two sets of coefficients generally differ by no more than 1%–2%, suggesting that the aug-cc-pVQZ +$(3s3p2d)$ basis set is nearly saturated. Truncating the one-electron basis set seems to have the largest effect on the isotropic coefficient $A_{0,0,0}$ computed at small values of R, where the potential energy surface is strongly repulsive.

TABLE II. Angular expansion coefficients $A_{l_1,l_2,L}(R, r_1, r_2)$, in cm^{-1}, computed from aug-cc-pVTZ and aug-cc-pVQZ *ab initio* energies. A $(3s3p2d)$ set of bond functions is used in all calculations. The coefficients are grouped into pairs of rows corresponding to fixed (R, r_1, r_2); the upper row in each pair lists the aug-cc-pVQZ coefficients, while the lower row in each pair lists the aug-cc-pVTZ coefficients. These coefficients do not include the full-triples correction.

R (a_0)	(r_1, r_2) (a_0)	$A_{0,0,0}$	$A_{2,0,2}$	$A_{0,2,2}$	$A_{2,2,4}$
4.5	(1.1, 1.1)	378.145	10.026	10.026	6.360
		382.457	10.094	10.094	6.320
4.5	(1.4, 1.4)	570.418	19.989	19.989	14.277
		576.072	20.116	20.116	14.197
4.5	(1.7, 1.7)	776.340	31.141	31.141	24.607
		783.772	31.379	31.379	24.478
4.5	(1.1, 1.7)	573.576	11.959	33.199	13.032
		579.204	11.878	33.480	13.044
5.0	(1.1, 1.1)	101.523	3.023	3.023	3.607
		103.343	3.046	3.046	3.585
5.0	(1.4, 1.4)	174.837	6.794	6.794	8.119
		177.554	6.879	6.879	8.070
5.0	(1.7, 1.7)	262.487	11.883	11.883	14.347
		266.336	12.043	12.043	14.254
5.0	(1.1, 1.7)	178.370	3.853	12.040	7.370
		181.142	3.883	12.179	7.325
6.5	(1.4, 1.4)	−22.530	−0.543	−0.543	2.070
		−22.239	−0.528	−0.528	2.054

C. CCSDT *ab initio* calculations

Our earlier study of the vibrational dependence of the H_2-H_2 interaction[38] indicates that incompleteness in the many-electron basis set could materially affect the shape of the potential energy surface in the van der Waals well. Similar effects have been observed in other weakly bound dimers of two-valence-electron systems.[39,40] To reduce the error associated with truncation of the many-electron basis set at the CCSD(T) level of theory, we employ a coupled-cluster treatment that includes a fully iterative treatment of single, double, and triple excitations,[41,42] abbreviated CCSDT, to compute the H_2-H_2 interaction energy at selected high-symmetry geometries (those in which θ_1, θ_2, and ϕ take values of 0 or $\pi/2$). These calculations are performed using the tensor contraction engine[43] incorporated into Version 4.7 of the electronic structure code NWCHEM.[44,45]

Unfortunately, the CCSDT calculations are prohibitively expensive if we employ the aug-cc-pVQZ+$(3s3p2d)$ one-electron basis set used in the CCSD(T) calculations. We, therefore, perform the CCSDT calculations using a smaller one-electron basis set consisting of only atom-centered aug-cc-pVTZ functions. We also use NWCHEM to perform CCSD(T) calculations at these high-symmetry geometries using the atom-centered aug-cc-pVTZ basis set. We then take the difference between the CCSDT and CCSD(T) counterpoise-corrected interaction energies as an additive correction to the aug-cc-pVQZ+$(3s3p2d)$ CCSD(T) potential energy surface. For the sake of brevity, we will call this the "full-triples" correction. We found that to ensure convergence of the CCSDT iterations at some geometries, it was necessary to increase the cutoff for computational linear dependence in the one-electron basis set to 10^{-6}. For consistency, we therefore used this cutoff in all of the CCSDT and CCSD(T) calculations performed with NWCHEM.

Because we compute the full-triples correction at a small number of H_2-H_2 orientations $(\theta_1, \theta_2, \phi)$, we cannot use the quadrature scheme described in the the previous subsection to extract corresponding full-triples corrections to the $A_{l_1,l_2,L}$ coefficients computed at the CCSD(T) aug-cc-pVQZ +$(3s3p2d)$ level of theory. Instead, we use least-squares techniques to fit the full-triples correction to the function

$$\Delta A_{0,0,0}(R,r_1,r_2)G_{0,0,0}(\theta_1,\theta_2,\phi)$$
$$+ \Delta A_{0,2,2}(R,r_1,r_2)G_{0,2,2}(\theta_1,\theta_2,\phi)$$
$$+ \Delta A_{2,0,2}(R,r_1,r_2)G_{2,0,2}(\theta_1,\theta_2,\phi)$$
$$+ \Delta A_{2,2,4}(R,r_1,r_2)G_{2,2,4}(\theta_1,\theta_2,\phi). \tag{6}$$

We then add the corrections $\Delta A_{l_1,l_2,L}$ to the corresponding coefficients $A_{l_1,l_2,L}$ obtained from four-dimensional quadrature over the CCSD(T) aug-cc-pVQZ+$(3s3p2d)$ interaction energies. The CCSDT and CCSD(T) energies used to compute the full-triples correction are available through EPAPS.[36] For the sake of brevity, we henceforth use the term "coefficients" to mean the sum of the CCSD(T) coefficients and the full-triples corrections.

D. Construction of a smooth potential energy surface

We now construct a smooth potential energy surface from the *ab initio* coefficients $A_{l_1,l_2,L}(R,r_1,r_2)$. For each pair of H_2 bond lengths (r_1,r_2), we create four cubic splines, one for each of the coefficients $A_{l_1,l_2,L}$, that interpolate the 19 coefficient values between $R=4.25a_0$ and $R=12.0a_0$. We extrapolate the splines to R values below $4.25a_0$ and above $12.0a_0$ using functions described in the next two paragraphs. At $R=4.25a_0$, the slope of each cubic spline is constrained to match the slope of the corresponding small-R extrapolating function.

We extend each cubic spline to R values below $4.25a_0$ using a simple two-parameter exponential extrapolation of the form $U\exp(-cR)$ that fits the coefficients obtained at $R=4.25a_0$ and $4.5a_0$. We should stress that this extrapolation is *not* expected to give highly accurate interaction energies for small R; we use it simply to define the slope for the cubic spline at $R=4.25a_0$. The dimer bound state wave functions we compute using our potential energy surface are not sensitive to the highly repulsive small-R region of the potential energy surface.

Beyond $R=12.0a_0$, we extrapolate each spline using an inverse-power expansion of the form $\Sigma_n C_n/R^n$, including terms with $n=5$ and 6 in the extrapolations for $A_{2,2,4}$, terms with $n=6$, 8, and 10 for $A_{0,0,0}$, and terms with $n=6$ and 8 in the extrapolations for $A_{0,2,2}$ and $A_{2,0,2}$. All C_n coefficients are determined as functions of r_1 and r_2. The C_5 coefficient for $A_{2,2,4}$ is computed from the H_2 quadrupole moments listed in Ref. 46. The C_6 coefficients are obtained from the isotropic and anisotropic R^{-6} dispersion energy coefficients given in Ref. 47 and the expressions given in Ref. 48. The C_8 and C_{10} dispersion energy coefficients are obtained from Ref. 49.

To reduce the discontinuities in the higher-order derivatives of the coefficients at $R=12.0a_0$, where the cubic spline meets the long-range inverse-power extrapolating function, we use the long-range function to compute values of the $A_{l_1,l_2,L}$ coefficients at six evenly spaced "phantom" points ranging from $R=13.0a_0$ to $R=18.0a_0$, and force the spline to intercept these phantom points as well as the points computed at the 19 R values cited above. At $R=18.0a_0$, we also constrain the slope of the spline to match that of the inverse-power expansion. However, we only use the spline to evaluate the coefficients between $R=4.25a_0$ and $R=12.0a_0$; beyond $R=12.0a_0$, we use the inverse-power expansion to compute the coefficients $A_{l_1,l_2,L}$.

Using these extrapolated cubic splines, we can compute the coefficients $A_{l_1,l_2,L}(R,r_1,r_2)$ at any R for the discrete pairs of H_2 bond lengths (r_1,r_2) at which we performed the *ab initio* calculations described above. As the last step in defining a smooth potential energy surface, we fit these interpolated (or extrapolated) coefficients to the expression

$$\sum_{k=0}^{2}\sum_{n=0}^{2} c_{k,n}(r_1-r_{eq})^k(r_2-r_{eq})^n, \tag{7}$$

where $r_{eq}=1.4a_0$.

Figure 1 shows how the isotropic coefficient $A_{0,0,0}(R,r_1,r_2)$, vibrationally averaged over the ground-state vibrational wave functions of the two H_2 monomers, depends
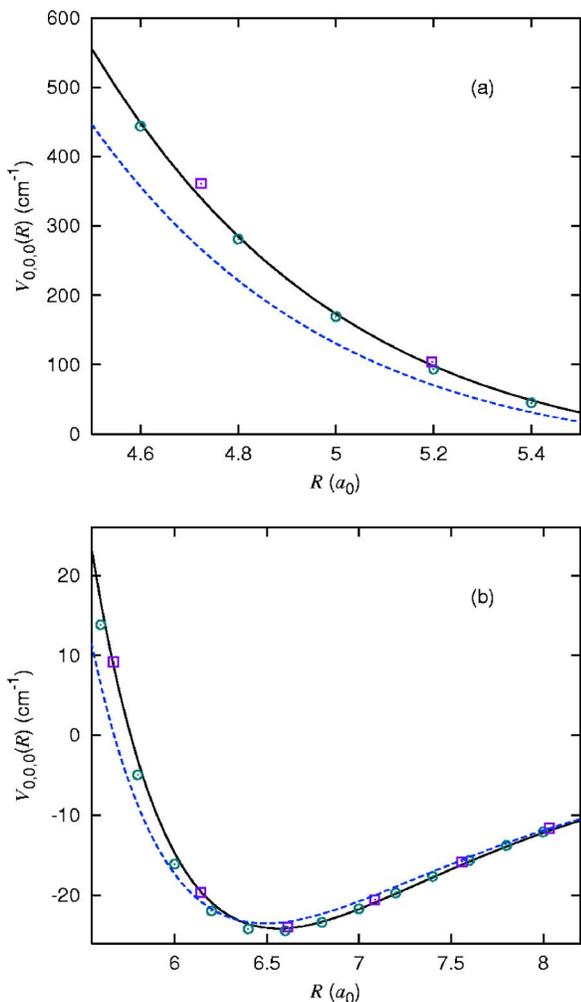
FIG. 1. (Color online) Comparison of the vibrationally averaged isotropic H$_2$–H$_2$ potential energy curve $A_{0,0,0}(R)$ obtained in this work (solid line) with the isotropic rigid-rotor potential energy curves obtained by other researchers. Boxes represent the extrapolated CCSD(T) potential energy surface of Ref. 14; circles represent the adjusted *ab initio* potential of Ref. 17; the dashed line represents the empirical potential of Ref. 50. The solid line shown here is computed from the unmodified $(s,q) = (0,0)$ potential energy surface. Panel (a) shows the repulsive wall at small-R values; panel (b) shows the van der Waals well.

on R both in the small-R, repulsive region of the potential energy surface and in the shallow H$_2$–H$_2$ well. We compare the vibrationally averaged $A_{0,0,0}$ coefficient computed in this work with a modified *ab initio* potential energy surface[17] that gives accurate predictions for the low-temperature second virial coefficient of H$_2$ gas, with the extrapolated CCSD(T) *ab initio* calculations of Diep and Johnson,[14] and with an empirical isotropic potential energy curve[50] obtained from an analysis of the total scattering cross section of moderate energy H$_2$–D$_2$ collisions.

In the shallow well, our vibrationally averaged $A_{0,0,0}$ coefficient agrees fairly well with the extrapolated CCSD(T) results,[14] which were computed within the rigid-rotor approximation using the $v = 0$ vibrationally averaged bond length for both H$_2$ monomers. The repulsive wall of our isotropic potential energy curve is slightly softer than that of the extrapolated CCSD(T) curve; our repulsive wall closely tracks the shape of the modified *ab initio* potential energy

surface[17] that gives accurate second virial coefficients, except that our repulsive wall is shifted to slightly larger R values. It is interesting to note that in the small-R repulsive region, the empirical isotropic potential energy curve[50] derived from scattering data is considerably softer than any of the three curves derived from *ab initio* computations.

III. COMPUTATION OF DIMER BOUND STATE ENERGIES

We assess the quality of our potential energy surface by using it to compute the energies of several bound (and long-lived quasibound) states of the (H$_2$)$_2$, H$_2$–D$_2$, and (D$_2$)$_2$ dimers. In this section, we summarize the methods used to compute these energies; the energies themselves are presented in later sections. We employ a standard close-coupled approach[29] in which the nine-dimensional dimer wave function is written as

$$\Psi(\mathbf{R}, \mathbf{r}_1, \mathbf{r}_2)$$
$$= R^{-1} \sum_\lambda F_\lambda(R) I_{J,M,\gamma}(\hat{\mathbf{R}}, \hat{\mathbf{r}}_1, \hat{\mathbf{r}}_2) \phi_{v_1,j_1}(r_1) \phi_{v_2,j_2}(r_2). \quad (8)$$

Here $\mathbf{r}_i$ is the vector separating the two nuclei of H$_2$ molecule i, $\mathbf{R}$ is the vector separating the two molecules' centers of mass, and $\hat{\mathbf{r}}_i$ and $\hat{\mathbf{R}}$ are the corresponding unit vectors. The quantum numbers J and M represent, respectively, the total angular momentum of the dimer (excluding nuclear spin angular momentum) and its projection on a space-fixed z axis. The angular basis functions $I_{J,M,\gamma}$, which are defined as

$$I_{J,M,\gamma}(\hat{\mathbf{R}}, \hat{\mathbf{r}}_1, \hat{\mathbf{r}}_2)$$
$$= \sum_{m_1,m_2,M_{12},N} C(j_1, m_1, j_2, m_2; J_{12}, M_{12})$$
$$\times C(J_{12}, M_{12}, L, N; J, M) Y_{j_1,m_1}(\hat{\mathbf{r}}_1)$$
$$\times Y_{j_2,m_2}(\hat{\mathbf{r}}_2) Y_{L,N}(\hat{\mathbf{R}}), \quad (9)$$

couple the rotational angular momenta (j_1, j_2) of the two H$_2$ molecules with the orbital angular momentum L of the dimer to create functions of definite J and M; we use γ to represent the collection of angular momentum quantum numbers (j_1, j_2, J_{12}, L), where J_{12} is the quantum number corresponding to the (vector) sum of the rotational angular momenta of the two H$_2$ molecules. The summation index λ represents a collection of eight quantum numbers: The four quantum numbers listed in γ, the total angular momentum quantum numbers J and M, and the vibrational quantum numbers v_1 and v_2 of the two monomers. The functions $\phi_{v,j}(r)$ are H$_2$ monomer radial wave functions, defined so that

$$\int_0^\infty \phi_{v,j}^*(r) \phi_{v',j'}(r) dr = \delta_{v,v'} \delta_{j,j'} \quad (10)$$

and obtained from a Numerov-Cooley[51] analysis of the Kołos-Wolniewicz[52] H$_2$ potential energy curve.

The dimer radial functions $F_\lambda(R)$ are solutions to a set of coupled second-order differential equations; the R-dependent terms that couple the radial functions $F_\lambda(R)$ and $F_{\lambda'}(R)$ are obtained by integrating the six-dimensional H$_2$–H$_2$ potential

TABLE III. Monomer spectroscopic constants (in cm^{-1}) and total masses employed in the dimer bound state calculations.

Species	$\Delta E\ (v=1 \leftarrow 0)$	$B\ (v=0)$	$B\ (v=1)$	Mass (m_e)
H_2	4161.169	59.0622	56.1117	3674.3
D_2	2993.614	29.8445	28.7908	7342.9

energy surface over the eight coordinates $(\mathbf{r}_1, \mathbf{r}_2, \hat{\mathbf{R}})$, and are defined by replacing the rigid-rotor potential coefficients $A_{l_1,l_2,L}(R)$ in Eq. (9) of Ref. 29 with the corresponding vibrationally averaged coefficients

$$\langle v_1, j_1; v_2, j_2 | A_{l_1,l_2,L}(R, r_1, r_2) | v'_1, j'_1; v'_2, j'_2 \rangle$$

$$= \int_0^\infty \int_0^\infty \phi^*_{v_1,j_1}(r_1) \phi^*_{v_2,j_2}(r_2) A_{l_1,l_2,L}(R, r_1, r_2)$$

$$\times \phi_{v'_1,j'_1}(r_1) \phi_{v'_2,j'_2}(r_2) dr_1 dr_2. \qquad (11)$$

We use the ABVN program[53] to evaluate the angular momentum coupling coefficients that appear in Eq. (9) of Ref. 29.

We convert the set of coupled second-order differential equations to a matrix eigenproblem by discretizing the equations on a grid in R, ranging from $R_{min} = 3.0a_0$ to $R_{max} = 48.0a_0$ in steps of $0.2a_0$, and replacing the dimer radial kinetic energy operator with a five-point central difference approximation evaluated on the grid. (Convergence tests show that using a smaller step size or a larger value of R_{max} does not change significantly the energies of the dimer states considered here.) We then solve the matrix eigenproblem using the ARPACK code[54] driven by the SYMMLQ linear algebra routine.[55] We truncate the wave function expansion given in Eq. (8) by limiting j_1 and j_2 to the values 0, 2, and 4, with the additional restriction that $j_1 + j_2 \leq 6$, and by limiting v_1 and v_2 to the values 0 and 1. We also assume that the three vibrational manifolds defined by $v_t = v_1 + v_2 = 0$, 1, or 2 are effectively decoupled from one another, which further reduces the size of the matrix eigenproblem. The energies of the (v, j) rovibrational states of the H_2 and D_2 monomers and the dimer reduced masses, which appear in the close-coupled equations for the radial functions $F_\lambda(R)$, are computed from the parameters listed in Table III.

Because we consider only even values of j_1 and j_2 here, the parity of the angular basis function $I_{J,M,\gamma}$ is controlled by the dimer orbital angular momentum quantum number L; when L is even, $I_{J,M,\gamma}$ has even parity. Angular basis functions with different parities are not coupled together by Eq. (8). In addition, for a dimer of two identical monomers, the overall spatial wave function (exclusive of spin) must be either symmetric or antisymmetric under exchange of the two monomers, and the overall spin wave function must also be symmetric or antisymmetric under monomer exchange. The total wave function, which is the product of the spatial and spin wave functions, must be symmetric or antisymmetric under monomer exchange for bosonic and fermionic monomers, respectively.

The para-H_2 molecule is a spin-zero composite boson. For a dimer of such bosons, no exchange-antisymmetric spin wave function can be constructed, and therefore only states whose spatial wave functions are symmetric under monomer exchange are physically admissible. These exchange-symmetric spatial wave functions are the only $(H_2)_2$ wave functions considered here. On the other hand, ortho-D_2 molecules may have a total nuclear spin quantum number of either zero or 2, and it is possible to construct (ortho-$D_2)_2$ dimers that have either an exchange-symmetric or an exchange-antisymmetric spin wave function. Consequently the spatial wave function for (ortho-$D_2)_2$ may also be either symmetric or antisymmetric under monomer exchange, provided that the total (spin times spatial) (ortho-$D_2)_2$ wave function is symmetric under monomer exchange.[56]

To check that our matrix-based implementation of the close-coupled formalism is correct, we have used the BOUND code[57] to compute the energies of the $(H_2)_2$, H_2-D_2, and $(D_2)_2$ bound states that correlate with the monomers' $(v, j) = (0, 0)$ ground rovibrational states, and compare these energies with those obtained from our matrix-based code. [Because the BOUND code employs the rigid-rotor approximation, for this comparison we ignore the j dependence of the monomer radial wave functions $\phi_{v,j}(r)$ that appear in Eq. (8) and replace these radial wave functions with those for the monomers' ground rovibrational states. This is equivalent to neglecting centrifugal distortion effects on the monomer radial wave functions.] The good agreement between these two calculations confirms the validity of our matrix-based close-coupled approach.

Some of the dimer states discussed below are long-lived quasibound states that can decay via rotational predissociation. The energies reported for these states are those obtained following the "infinite wall" procedure outlined by Grabenstetter and Le Roy,[58] in which the energy of the quasibound state is monitored as R_{max} is decreased in $0.2a_0$ steps. We estimate that using a finite step size of $0.2a_0$ in this procedure introduces an uncertainty in the quasibound state energies of no more than $0.003\ cm^{-1}$.

IV. EMPIRICAL ADJUSTMENTS TO THE POTENTIAL ENERGY SURFACE

In this section, we show that if we make two small empirical modifications to our *ab initio* potential energy surface, it gives rotational and rovibrational transition energies for $(H_2)_2$, H_2-D_2, and $(D_2)_2$ dimers in good agreement with those obtained experimentally. The two modifications involve a small inward shift of the repulsive wall of the potential energy surface, which we quantify using an adjustable parameter s, and a slight increase in the magnitude of the surface's $A_{2,2,4}$ term, which we quantify using an adjustable parameter q. The unmodified, purely *ab initio* potential energy surface is defined by $(s, q) = (0, 0)$.

We focus first on H_2-D_2 and $(D_2)_2$ dimer states that correlate with rotationally cold $(j = 0)$ monomers as $R \to \infty$. Because the wave functions of these states are overwhelmingly dominated by angular basis functions $I_{J,M,\gamma}$ with $j_1 = j_2 = 0$ in Eq. (8), the states' energies are insensitive to the anisotropic terms $(A_{0,2,2}, A_{2,0,2},$ and $A_{2,2,4})$ of the potential energy surface; however, the states' energies are very sensitive to the location of the surface's repulsive wall. We there-

fore find the optimal value for s by adjusting s to bring the computed energies for transitions involving these states into good agreement with experimentally measured transition energies.

Next, we consider IR-active transitions of the H$_2$–D$_2$ dimer which involve either (1) a pure vibrational transition $v=1\leftarrow0$ in the H$_2$ monomer and a pure rotational transition $j=2\leftarrow0$ in the D$_2$ monomer or (2) a rovibrational transition $(v,j)=(1,2)\leftarrow(0,0)$ in the H$_2$ monomer and no excitation of the D$_2$ monomer. These transitions involve final states whose energies are sensitive to the $A_{0,2,2}$ and $A_{2,0,2}$ anisotropic terms of the dimer potential energy surface. We find that, once the repulsive wall of the potential energy surface has been shifted inward slightly, the energies computed for these transitions are in good agreement with experimental measurements. This suggests that the $A_{0,2,2}$ and $A_{2,0,2}$ terms of the shifted potential energy surface are accurate, at least in the range of R values probed by the H$_2$–D$_2$ dimer wave functions.

Finally, we examine (H$_2$)$_2$ and (D$_2$)$_2$ dimer states which correlate with $R\rightarrow\infty$ limits involving one $j=0$ and one $j=2$ molecule. Some of these states have energies that are very sensitive to the strength of the $A_{2,2,4}$ term of the potential energy surface. By examining how the computed energies for transitions involving these states change with q, we find the value for q that gives the best overall agreement with experimental measurements.

A. Combination differences from the H$_2$–D$_2$ and (D$_2$)$_2$ dimer $Q_1(0)$ infrared spectra

We begin by computing the $J=2\leftarrow0$ spacings for the H$_2$–D$_2$ and (D$_2$)$_2$ dimers that correlate with rotationally cold ($j=0$) monomers; we perform these computations both for the dimers' $v_t=0$ ground vibrational manifolds and for the $v_t=1$ manifold accessed by IR excitation of the H$_2$ monomer in the H$_2$–D$_2$ dimer. Accurate experimental values for these $J=2\leftarrow0$ spacings have been obtained from a combination-differences analysis of high-resolution H$_2$–D$_2$ and (D$_2$)$_2$ IR absorption spectra.[25] Because of the large energy mismatch between the $v=1$ levels of H$_2$ and D$_2$, in our calculations we assume that the H$_2$–D$_2$ dimer states correlating with H$_2(v=1)$+D$_2(v=0)$ are decoupled from those correlating with H$_2(v=0)$+D$_2(v=1)$. (Strictly speaking, the $v_t=1$ dimer states accessed in the IR absorption experiment are quasi-bound, and can decay through vibrational predissociation. Our assumption that these states are decoupled from the $v_t=0$ states, however, closes off this decay channel. Because the lifetimes of the $v_t=1$ dimer states are known to be extremely long,[25] this should not materially affect our results.)

Table IV shows that the computed $J=2\leftarrow0$ spacings are $0.015-0.025$ cm^{-1} lower than the experimental ones. If the dimers were rigid rotors, the $J=2\leftarrow0$ spacings would be equal to six times the dimers' respective rotational constants. Because the dimers undergo large-amplitude zero-point motion along the R direction, a rigid-rotor model for the dimers' overall end-over-end rotation is not really appropriate. Nonetheless, this simple-minded picture suggests that the dimer states supported by the computed potential energy surface

TABLE IV. Observed and computed spacings (in cm^{-1}) between the $J=0$ and $J=2$ states of H$_2$–D$_2$ and D$_2$–D$_2$ dimers that correlate with $j=0$ states of the constituent monomers. These bound state computations employ the unmodified $(s,q)=(0,0)$ potential energy surface.

Dimer	Observed	Computed
H$_2(v=0)$+D$_2(v=0)$	3.848	3.816
H$_2(v=1)$+D$_2(v=0)$	3.889	3.862
D$_2(v=0)$+D$_2(v=0)$	3.001	2.986

have average intermolecular distances that are slightly too large, by about $0.02a_0$ for the (D$_2$)$_2$ dimer and $0.03a_0$ for the H$_2$–D$_2$ dimer.

As we noted in our discussion of Fig. 1, a small inward shift of the repulsive wall of our potential energy surface would bring it into closer agreement with a surface[17] that gives accurate second virial coefficients for low-temperature H$_2$ gas; such a shift would also reduce slightly the average intermolecular distances of the H$_2$–D$_2$ and (D$_2$)$_2$ dimers, possibly bringing the computed $J=2\leftarrow0$ spacings into better agreement with experiment. (We note here that the potential energy surface presented in Ref. 17 was itself obtained by a similar inward shift of the repulsive wall of an *ab initio* computed potential energy surface.) We therefore modify our *ab initio* H$_2$–H$_2$ potential energy surface as follows. For R values below $6.5a_0$, we shift our computed *ab initio* interaction energies to new, smaller, R values defined by

$$R_{\mathrm{new}} = R_{\mathrm{old}} - s(6.5a_0 - R_{\mathrm{old}}), \qquad (12)$$

and then construct a smooth s-dependent H$_2$–H$_2$ potential energy surface (as described above in Sec. II D) using the shifted points. Because we have not yet changed the strength of the $A_{2,2,4}$ term, we are at present implicitly holding q fixed at $q=0$.

Figure 2 shows how the errors in the $J=2\leftarrow0$ spacings computed for the H$_2$–D$_2$ and (D$_2$)$_2$ dimers change as s increases from $s=0$ to $s=0.025$. Choosing $s=0.0175$ brings all three of these computed spacings into agreement with ex-
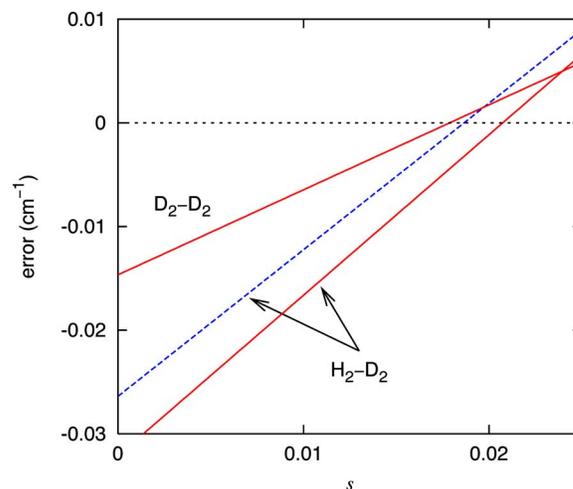

FIG. 2. (Color online) Dependence on s of the errors (computed minus experiment) in the $J=2\leftarrow0$ spacings of the H$_2$–D$_2$ and (D$_2$)$_2$ dimers. Solid lines are for the vibrationally cold ($v_t=0$) dimers; the dashed line is for the H$_2$ $(v=1)$+D$_2$ $(v=0)$ dimer. The parameter q is held fixed at $q=0$.

TABLE V. Observed transition energies and deviations between observed and computed transition energies (computed minus experiment), in cm^{-1}, for selected IR-active transitions of the H_2-D_2 dimer involving $v=1\leftarrow0$ excitation of the H_2 monomer. The D_2 monomer remains in its $v=0$ vibrational level during the transition. The initial and final states are identified by the angular momentum quantum numbers associated with the dominant term in the dimer wave function [Eq. (8)]; j_1 and j_2 are the angular momenta of the H_2 and D_2 molecules, respectively. The computed transition energies are obtained using the $(s,q)=(0.0175,0)$ potential energy surface.

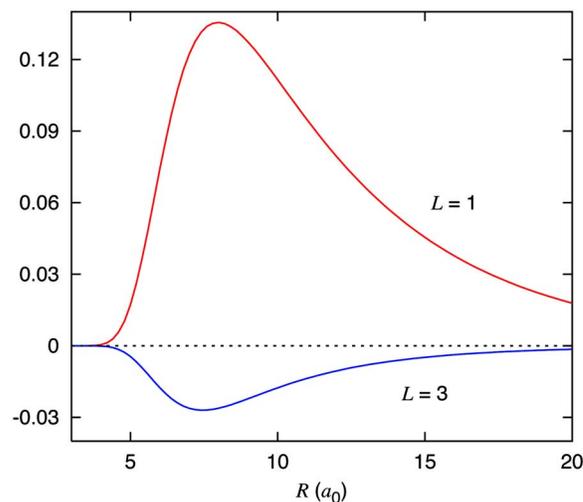| $(J,L,j_1,j_2)'\leftarrow(J,L,j_1,j_2)''$	Observed	Deviation
$(1,1,0,2)\leftarrow(2,2,0,0)$	4337.046	+0.007
$(2,1,0,2)\leftarrow(2,2,0,0)$	4337.609	+0.006
$(0,2,0,2)\leftarrow(1,1,0,0)$	4342.004	+0.011
$(1,2,0,2)\leftarrow(1,1,0,0)$	4342.208	+0.006
$(1,1,2,0)\leftarrow(2,2,0,0)$	4494.719	+0.001
$(2,1,2,0)\leftarrow(2,2,0,0)$	4495.20	+0.015

FIG. 3. (Color online) The two dominant $F_\lambda(R)$ radial functions for the $(J,L)=(1,1)$ upper state accessed in the $(H_2)_2$ dimer's $S_0(0)$ IR transition. These functions are computed using the $(s,q)=(0.0175,0)$ potential energy surface.

periment. Fixing s at this value amounts to an inward shift of the crossing point R_0, where the vibrationally averaged H_2-H_2 isotropic coefficient $A_{0,0,0}(R)=0$, from $R_0=5.775a_0$ for the original *ab initio* potential energy surface (with $s=0$) to $R_0=5.762a_0$ for the empirically modified surface. The corresponding shift for the H_2-D_2 dimer is from $R_0=5.773a_0$ to $R_0=5.760a_0$; for the $(D_2)_2$ dimer, the shift is from $R_0=5.769a_0$ to $R_0=5.756a_0$.

B. $Q_1(0)+S_0(0)$ and $S_1(0)$ infrared spectra of the H_2-D_2 dimer

Next, we consider transitions of the H_2-D_2 dimer in which either (1) the H_2 monomer undergoes a pure $v=1\leftarrow0$ vibrational transition and the D_2 monomer simultaneously makes a pure $j=2\leftarrow0$ rotational transition or (2) the H_2 monomer undergoes the rovibrational transition $(v,j)=(1,2)\leftarrow(0,0)$ while the D_2 monomer remains in its rovibrational ground state. The former transitions belong to the dimer's $Q_1(0)$ [H_2]$+S_0(0)$ [D_2] band, and the latter transitions to the dimer's $S_1(0)$ [H_2] band; for brevity, in this subsection we henceforth drop the molecular labels in square brackets and simply refer either $Q_1(0)+S_0(0)$ or $S_1(0)$ transitions.

Because of the large energy mismatch between the $j=2$ states of the H_2 and D_2 molecules, the upper states involved in these transitions are ones in which the $j=2$ excitation remains localized on one of the monomers, and thus have energies that are insensitive to the $A_{2,2,4}$ term of the potential energy surface. The computed energies for these transitions consequently provide insight into the quality of the surface's $A_{0,0,0}$, $A_{0,2,2}$, and $A_{2,0,2}$ terms.

Four relatively sharp $Q_1(0)+S_0(0)$ transitions and two relatively sharp $S_1(0)$ transitions have been observed in the IR absorption spectrum of the H_2-D_2 dimer.[25] As Table V shows, the potential energy surface with $s=0.0175$ gives transition energies for these six transitions in very good agreement with the experiment; this suggests that the surface's $A_{0,2,2}$ and $A_{2,0,2}$ terms are fairly accurate, at least over the range of R values for which the H_2-D_2 dimer has substantial probability density.

C. $S_0(0)$ infrared spectra of the $(H_2)_2$ and $(D_2)_2$ dimers

Finally we consider IR-active transitions of the $(H_2)_2$ and $(D_2)_2$ dimers that correlate with the $S_0(0)$ $j=2\leftarrow0$ pure rotational transitions of the H_2 and D_2 monomers. The upper states involved in these transitions are ones in which the $j=2$ excitation is shared by the two monomers; the energies of these states are therefore sensitive to the $A_{2,2,4}$ term of the dimer potential energy surface, which couples together angular functions in Eq. (8) with $(j_1,j_2)=(0,2)$ and $(j_1,j_2)=(2,0)$.

Because of the low reduced mass of the $(H_2)_2$ dimer and the restrictions imposed by nuclear spin statistics, there is just one sharp $S_0(0)$ IR-active transition for this dimer; it is a $(J,L)=(1,1)\leftarrow(0,0)$ transition and appears in the $(H_2)_2$ far-IR absorption spectrum at 355.425 cm^{-1}.[27] The transition energy computed for this absorption feature using the $(s,q)=(0.0175,0)$ potential energy surface is 355.438 cm^{-1}, or 0.013 cm^{-1} too high.

The dimer wave function [Eq. (8)] for the upper state of this transition contains significant contributions from only four channels: Those with (j_1,j_2,J_{12},L) angular momentum quantum numbers of $(0,2,2,1)$, $(0,2,2,3)$, $(2,0,2,1)$, and $(2,0,2,3)$. Furthermore, only two of these channels give independent contributions to the wave function; for the $(H_2)_2$ dimer, exchange symmetry constraints force the channels with $(j_1,j_2,J_{12},L)=(a,b,J_{12},L)$ and $(j_1,j_2,J_{12},L)=(b,a,J_{12},L)$ to, when L is odd, have radial functions $F_\lambda(R)$ that are equal in magnitude but opposite in sign. Figure 3 shows the $F_\lambda(R)$ radial functions for the two independent channels $(j_1,j_2,J_{12},L)=(0,2,2,1)$ and $(0,2,2,3)$ that define the upper state of the $(J,L)=(1,1)\leftarrow(0,0)$ transition; about 97% of the upper state's probability density is associated with the two $L=1$ channels.

If we compute the expectation value of the dimer's potential energy using the upper-state wave function,
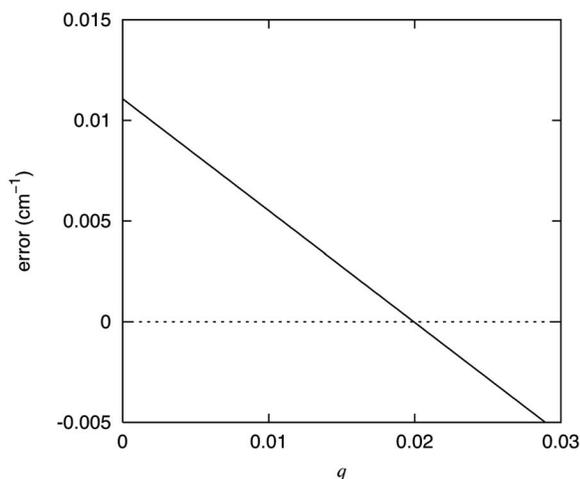
FIG. 4. Dependence on q of the error (computed minus experiment) in the transition energy computed for the (H$_2$)$_2$ dimer's far-IR $S_0(0)$ absorption feature. The parameter s is held fixed at $s=0.0175$.

$$\langle V \rangle = \int \int \int |\Psi(\mathbf{R},\mathbf{r}_1,\mathbf{r}_2)|^2 V(\mathbf{R},\mathbf{r}_1,\mathbf{r}_2)d\mathbf{R}d\mathbf{r}_1 d\mathbf{r}_2, \quad (13)$$

we find that it includes substantial contributions from the isotropic $A_{0,0,0}$ term of the potential surface and the anisotropic $A_{0,2,2}$ and $A_{2,0,2}$ terms, along with a small contribution from the $A_{2,2,4}$ term; this last contribution is proportional to the integral

$$\int_0^\infty F_\lambda(R)F_{\lambda'}(R)dR, \quad (14)$$

where F_λ and $F_{\lambda'}$ are the two radial functions shown in Fig. 3. As we explained previously, the lower state for this transition has a wave function dominated by the $(j_1,j_2)=(0,0)$ channel, and its potential energy expectation value is therefore, sensitive to only the isotropic $A_{0,0,0}$ term.

This analysis suggests that a small perturbation of the $A_{2,2,4}$ term will change the energy of the upper state, but not that of the lower state, and could thus bring the computed transition energy for this far-IR absorption feature into better agreement with experiment. Furthermore, because the transitions considered in the preceding two subsections involve states whose energies are insensitive to $A_{2,2,4}$, such a perturbation would preserve the good agreement with experiment observed for those transitions. (Naturally, we could also change the computed transition energy for this particular far-IR absorption feature by adjusting the $A_{0,2,2}$ and $A_{2,0,2}$ terms in the potential energy surface; however, such an adjustment would have the undesirable side effect of changing the transition energies computed in the immediately preceding subsection.) Here we adopt a very simple adjustment of the $A_{2,2,4}$ term, which helps compensate for the fact that the $A_{2,2,4}$ coefficients computed in Sec. II A include unwanted contributions from the electrostatic QH interaction: We multiply the $A_{2,2,4}$ coefficients computed at each of the 19 R values by the quantity $(1+q)$, where q is an adjustable parameter, and then reconstruct the entire potential energy surface as described in Sec. II D.

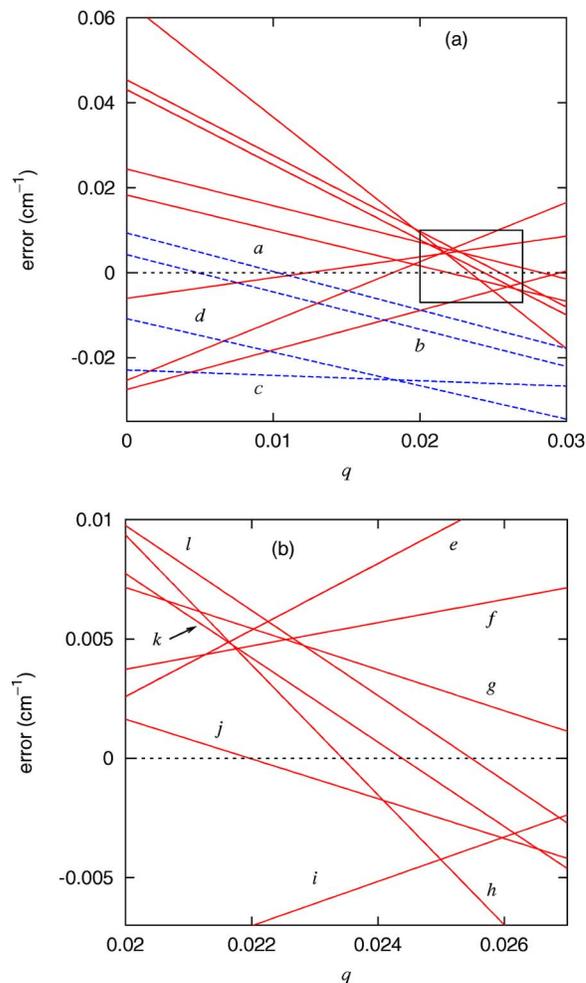Figure 4 shows how q changes the computed position of

FIG. 5. (Color online) Dependence on q of the errors (computed minus experiment) in the transition energies computed for 12 features in the (D$_2$)$_2$ dimer's far-IR $S_0(0)$ absorption band. Panel (b) is a magnification of the small box in panel (a). The labels affixed to each line refer to Table VI. The parameter s is held fixed at $s=0.0175$.

the (H$_2$)$_2$ dimer's $(J,L)=(1,1) \leftarrow (0,0)$ $S_0(0)$ far-IR absorption feature. At $q=0.02$, the computed transition energy coincides with the experimental value of 355.425 cm^{-1}. (However, the uncertainty of ± 0.005 cm^{-1} in this experimental transition energy means that a wide range of q values would be compatible with the experimental observations.) This suggests that a simple rescaling of our $A_{2,2,4}$ coefficients removes much of the QH interaction's erroneous contribution to these coefficients, even though the QH interaction has a different power-law dependence on R than does the quadrupole-quadrupole interaction that dominates the $A_{2,2,4}$ term.

To place tighter constraints on q, we turn to the (D$_2$)$_2$ dimer, which, because it is heavier than (H$_2$)$_2$ and has less severe restrictions arising from nuclear spin statistics, exhibits many more absorption features in its far-IR $S_0(0)$ band.[27] Twelve of these features are relatively sharp, suggesting that they involve bound or long-lived quasibound states, and also have firmly assigned initial- and final-state angular momentum quantum numbers. (We discuss later a 13th sharp transition whose initial- and final-state assignments are more tentative.) Figure 5 and Table VI show how the errors in the

TABLE VI. Observed transition energies and deviations between observed and computed transition energies (computed minus experiment), in cm^{-1}, for IR-active $(D_2)_2$ transitions in the D$_2$ $S_0(0)$ band. The computed transition energies are obtained using either the $(s,q)=(0.0175,0)$ or the $(s,q)=(0.0175,0.0235)$ potential energy surface.

Label	$(J,L)' \leftarrow (J,L)''$	Observed	Deviation $q=0$	Deviation $q=0.0235$
a	$(2,2)\leftarrow(3,3)$	175.507	+0.010	−0.012
b	$(2,2)\leftarrow(1,1)$	180.322	+0.005	−0.016
c	$(2,1)\leftarrow(2,2)$	177.359	−0.022	−0.026
d	$(3,3)\leftarrow(2,2)$	181.287	−0.010	−0.029
e	$(1,2)\leftarrow(1,1)$	182.328	−0.025	+0.007
f	$(1,3)\leftarrow(0,0)$	184.536	−0.006	+0.005
g	$(2,0)\leftarrow(3,3)$	172.776	+0.024	+0.004
h	$(0,2)\leftarrow(1,1)$	177.996	+0.064	+0.000
i	$(2,3)\leftarrow(2,2)$	182.797	−0.027	−0.005
j	$(2,0)\leftarrow(1,1)$	177.592	+0.018	−0.001
k	$(1,1)\leftarrow(0,0)$	178.747	+0.043	+0.002
l	$(1,1)\leftarrow(2,2)$	175.744	+0.045	+0.004

TABLE VII. Binding energies (in cm^{-1}) of selected $(H_2)_2$ dimer states that correlate with $j=0$ states of the constituent monomers. These bound state computations employ the $(s,q)=(0.0175,0.0235)$ potential energy surface.

v_t	J	Binding energy
0	0	2.895
1	0	3.300
1	1	1.559

transition.[27] Our potential energy surface predicts transition energies of 176.645 and 176.598 cm^{-1}, respectively, for these transitions.

Finally, we note that the computed transition energies listed in Table V change by only 0.001–0.002 cm^{-1} when the $(s,q)=(0.0175,0.0235)$ potential energy surface is used. This validates our decision to hold q fixed at $q=0$ while we find the optimal value for s, and then hold s fixed at this value while we find the optimal value for q.

V. OTHER COMPARISONS WITH EXPERIMENT

In the previous section, we showed that the quality of the four $A_{l_1,l_2,L}$ terms of our potential energy surface could be assessed individually by considering transitions between pairs of states that have energies sensitive to specific subsets of these terms. We found that with two small adjustments to the potential energy surface, we could generate a surface that gives computed transition energies in fairly good agreement with a number of high-resolution experimental measurements.

Although some of the transitions considered in the previous section involve vibrational excitation of the H$_2$ monomer in the H$_2$–D$_2$ dimer, we have not yet considered vibrationally excited states of the $(H_2)_2$ or $(D_2)_2$ dimers. In these dimers' $v_t=1$ vibrationally excited states, the vibrational excitation is delocalized across the pair of monomers; transitions to these excited states therefore probe the simultaneous dependence of the potential energy surface on r_1 and r_2.

In this section, we show that our modified potential energy surface predicts energies for these transitions that are in good agreement with the experiment, indicating that the surface accurately describes the vibrational coupling between the two monomers in the $(H_2)_2$ and $(D_2)_2$ dimers. We also consider IR-active *double* vibrational transitions of the $(D_2)_2$ dimer, in which each monomer undergoes a $v=1 \leftarrow 0$ excitation; the good agreement we obtain with the experiment pro-

energies computed for these 12 transitions depend on q. For the $q=0$ potential energy surface, the deviations between computed and measured transition energies range from −0.027 cm^{-1} (transition i) to +0.064 cm^{-1} (transition h); at $q=0.0235$, however, the computed energies for 8 of the 12 transitions (those labeled $e-l$) agree with the experiment to within ±0.007 cm^{-1}. Only one of these eight transitions has a computed transition energy that differs from the experimental value by more than 0.005 cm^{-1}, which is the experimental uncertainty quoted for these transitions in Ref. 27. Furthermore, the value $q=0.0235$ minimizes the mean absolute deviation between the predicted and observed transition energies for these eight transitions.

The four transitions labeled $a-d$ in Table VI exhibit poorer agreement with the experiment; furthermore, the errors in the computed energies for these four transitions at $q=0.0235$ are equal to or larger in magnitude than the errors at $q=0$. Transition c corresponds to a very weak far-IR absorption feature; inspection of Fig. 3 in Ref. 27 shows that its intensity is comparable to the level of background noise in the $(D_2)_2$ absorption spectrum, and it is possible that the true position of this feature differs slightly from that reported in Ref. 27. Transitions a, b, and d, however, correspond to relatively strong absorption features; furthermore, while transition a is a shoulder on the low-energy side of a very intense feature (transition l), transitions b and d are well isolated from other spectral features, and transitions a and b are linked by the $J=3 \leftarrow 1$ combination difference of the dimer's $j_1=j_2=0$ manifold. It seems unlikely that the quoted experimental uncertainties for these three transitions could be badly underestimated. It therefore appears that our potential energy surface slightly underpredicts the energies of the $(J,L)=(2,2)$ and $(3,3)$ excited-state levels accessed via these three IR transitions.

The experimental $(D_2)_2$ $S_0(0)$ IR absorption spectrum exhibits a 13th sharp feature, corresponding to the transition energy 176.627 cm^{-1}, which might be either the $(J,L)=(3,1)\leftarrow(2,2)$ transition or the $(J,L)=(3,2)\leftarrow(3,3)$

TABLE VIII. Binding energies (in cm^{-1}) of selected H$_2$–D$_2$ dimer states that correlate with $j=0$ states of the constituent monomers. These bound state computations employ the $(s,q)=(0.0175,0.0235)$ potential energy surface.

J	Vibrational state		
	$v_t=0$	$v=1$ (H$_2$)	$v=1$ (D$_2$)
0	4.417	4.792	4.644
1	3.074	3.442	3.299
2	0.574	0.905	0.779

TABLE IX. Binding energies (in cm^{-1}) of selected $(D_2)_2$ dimer states that correlate with $j=0$ states of the constituent monomers. The letters S and A indicate that the state is, respectively, symmetric or antisymmetric under monomer exchange. These bound state computations employ the $(s,q) = (0.0175, 0.0235)$ potential energy surface.

	Vibrational state		
J	$v_t=0$	$v_t=1$ (S)	$v_t=1$ (A)
0	6.712 (S)	7.118	6.939
1	5.696 (A)	5.925	6.101
2	3.711 (S)	4.111	3.941
3	0.885 (A)	1.109	1.263

vides further evidence that our modified potential energy surface has the correct (r_1, r_2) dependence.

A. $Q_1(0)$ spectra of the $(H_2)_2$, H_2-D_2, and $(D_2)_2$ dimers

Tables VII–IX list the energies of several $(H_2)_2$, H_2-D_2, and $(D_2)_2$ bound states that correlate with $j=0$ monomer states, computed using the final $(s,q) = (0.0175, 0.0235)$ potential energy surface. Using these bound state energies and the monomer $Q_1(0)$ transition energies from Table III, we can obtain theoretical positions for the P and R lines in the dimers' $Q_1(0)$ IR absorption spectra. In Table X, we list the computed positions for the 11 P and R lines that have been observed experimentally,[25] and compare the computed positions with the observed ones.

The computed transition energies for $(H_2)_2$ and H_2-D_2 are in good agreement with experiment, with the H_2-D_2 results deviating from the observed energies by amounts smaller than the estimated experimental uncertainties. The transition energies for $(D_2)_2$, however, deviate systematically from the experimental measurements by about -0.01 cm^{-1}, or about twice the estimated uncertainty in the measured transition energies.

To investigate this discrepancy further, we have computed the transition energies of the $(D_2)_2$ dimer's $P(2)$, $P(1)$, $R(0)$, and $R(1)$ lines using a set of potential energy surfaces with different s values, keeping q fixed at $q=0.0235$. (The P and R lines involving $J=3$ states have been omitted from this analysis simply because computing these states' energies at several values of s is very time consuming.) In Fig. 6 we show how the deviations between the computed and ob-
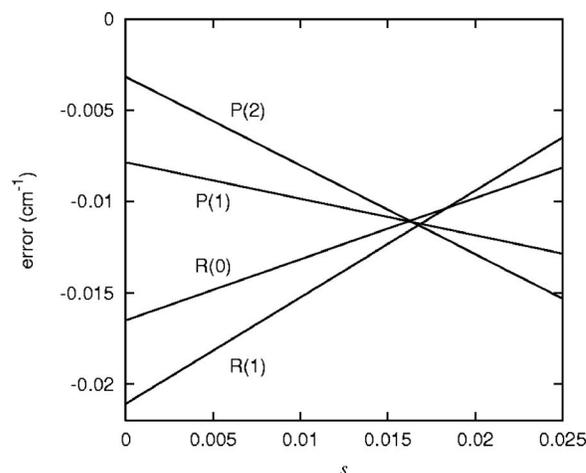

FIG. 6. Dependence on s of the errors (computed minus experiment) in the transition energies computed for four lines in the $(D_2)_2$ dimer's $Q_1(0)$ IR absorption band. The parameter q is held fixed at $q=0.0235$.

served transition energies change with s. Only for s values near 0.0175 do the computed transition energies deviate systematically from the experiment; in addition, the $s=0.0175$ energies listed in Table IX give $J=2\leftarrow0$ and $3\leftarrow1$ spacings for both the $v_t=0$ and IR-active $v_t=1$ manifolds within 0.002 cm^{-1} of the experimentally derived values.[25] These observations suggest that the systematic deviations observed for $(D_2)_2$ in Table X are not related to a poor choice for s.

These discrepancies could indicate a small error in the isotropic $A_{0,0,0}$ term's simultaneous dependence on r_1 and r_2; the vibrationally excited $(D_2)_2$ states involved in the transitions listed in Table X are antisymmetric linear combinations of $(v_1, v_2) = (0, 1)$ and $(1, 0)$ states and are therefore, sensitive to this (r_1, r_2) coupling. The same coupling term, however, is also active in the IR-active vibrationally excited $(H_2)_2$ state, and in the Raman-active $(H_2)_2$ excited state discussed in the next paragraph, and the agreement with experiment is excellent for transitions involving these states of the $(H_2)_2$ dimer. More work is needed to understand the systematic deviations in the final column of Table IX.

The $(H_2)_2$, H_2-D_2, and $(D_2)_2$ dimers should all have Raman-active transitions in the vicinity of the monomers' $Q_1(0)$ Raman transitions; thus far, however, only the $(H_2)_2$ dimer's Raman spectrum has been observed

TABLE X. Computed transition energies (in cm^{-1}) and deviations from experiment (computed minus experiment) of the P and R lines in the $Q_1(0)$ IR bands of the $(H_2)_2$, H_2-D_2, and $(D_2)_2$ dimers. For the H_2-D_2 dimer, the vibrationally excited state correlates with $v=1$ $H_2+v=0$ D_2; for the $(H_2)_2$ and $(D_2)_2$ dimers, the vibrational excitation is delocalized antisymmetrically across the two monomers. The computed transition energies are obtained using the $(s,q) = (0.0175, 0.0235)$ potential energy surface.

	$(H_2)_2$		H_2-D_2		$(D_2)_2$	
$J' \leftarrow J''$	Computed	Deviation	Computed	Deviation	Computed	Deviation
$2\leftarrow3$	⋯	⋯	⋯	⋯	2990.558	−0.007
$1\leftarrow2$	⋯	⋯	4158.301	+0.002	2991.400	−0.012
$0\leftarrow1$	⋯	⋯	4159.451	−0.001	2992.371	−0.011
$1\leftarrow0$	4162.505	−0.008	4162.144	−0.003	2994.401	−0.011
$2\leftarrow1$	⋯	⋯	4163.338	−0.003	2995.368	−0.011
$3\leftarrow2$	⋯	⋯	⋯	⋯	2996.216	−0.013

TABLE XI. Energies (in cm^{-1}) for $(H_2)_2$ states with $J_{12}=2$, $v_t=0$ or 1, and $L \leqslant 1$. The energies are obtained using the $(s,q)=(0.0175,0.0235)$ potential energy surface, and are given relative to the $S_0(0)$ and $S_1(0)$ H_2 monomer energies for $v_t=0$ and 1, respectively.

(J,L)	Energy $v_t=0$	Energy $v_t=1$
(1, 1)	−1.845	−2.008
(2, 0)	−3.022	−3.319
(2, 1)	−1.200	−1.470

experimentally.[28] It consists of a single narrow line corresponding to a transition energy of 4160.78 ± 0.02 cm^{-1}. The theoretical $Q_1(0)$ Raman transition energy for $(H_2)_2$ derived from the first two lines of Table VII is 4160.764 cm^{-1}; the difference between the computed and experimental Raman transition energies is only slightly smaller than the estimated experimental uncertainty. However, the reported value for the experimental Raman transition energy is based on a value of 4161.18 cm^{-1} for the $Q_1(0)$ transition of an isolated H_2 molecule. The difference between this value and the value used here (4161.169 cm^{-1}) accounts for more than half the difference between the computed and observed dimer Raman transition energies. If we, instead, compare the observed and computed dimerization-induced *redshift* of the H_2 $Q_1(0)$ Raman transition, we find that our computed redshift of 0.405 cm^{-1} is in excellent agreement with the reported value[28] of 0.400 ± 0.02 cm^{-1}.

B. $S_1(0)$ and $Q_1(0)+S_1(0)$ infrared spectra of the $(H_2)_2$ and $(D_2)_2$ dimers

We finally use our modified potential energy surface to compute transition energies for features in the $S_1(0)$ IR absorption bands of the $(H_2)_2$ and $(D_2)_2$ dimers, and for features in the $Q_1(0)+S_1(0)$ IR absorption band of the $(D_2)_2$ dimer. The $(D_2)_2$ transitions involve upper states whose energies are sensitive to the (r_1, r_2) dependence of the potential energy surface.

The $S_1(0)$ IR absorption spectrum of $(H_2)_2$ contains just one narrow line[25] at 4498.734 ± 0.004 cm^{-1}. This feature is associated with a transition from the dimer's ground state (the first line of Table V) to a state with $J=L=1$ that is a linear combination of $(v_1,j_1;v_2,j_2)=(1,2;0,0)$ and $(0,0;1,2)$; the final state's energy is listed in the first line of Table XI. The $(s,q)=(0.0175,0.0235)$ potential energy surface gives a computed $S_1(0)$ dimer transition energy of 4498.726 cm^{-1}, in good agreement with the observed value.

The angular basis functions $I_{J,M,\gamma}$ in Eq. (8) that correspond to $(J,L,j_1,j_2)=(1,1,0,2)$ and $(1,1,2,0)$, which dominate the final-state wave function for this $S_1(0)$ dimer transition, are not directly coupled together by any of the four terms $A_{l_1,l_2,L}$ that appear in our potential energy surface; consequently, this $(H_2)_2$ transition, like the H_2-D_2 transitions considered in Sec. IV B, probes primarily the *monomer* vibrational dependence of the surface's $A_{0,0,0}$, $A_{0,2,2}$, and $A_{2,0,2}$ terms. In contrast to the H_2-D_2 transitions discussed in Sec. IV B, however, the $(H_2)_2$ $S_1(0)$ transition is sensitive to the $A_{2,2,0}$ and $A_{2,2,2}$ terms of the potential energy surface, which

TABLE XII. Observed transition energies and deviations between observed and computed transition energies (computed minus experiment), in cm^{-1}, for IR-active $(D_2)_2$ transitions in the D_2 $S_1(0)$ band. The computed transition energies are obtained using the $(s,q)=(0.0175,0.0235)$ potential energy surface. The column labeled F indicates the fraction of upper-state probability associated with functions in Eq. (8) in which the $v=1$ and $j=2$ molecular excitations reside on the same monomer.

$(J,L)' \leftarrow (J,L)''$	Observed	Deviation	F
$(2,0) \leftarrow (1,1)$	3164.705	−0.005	0.984
$(1,1) \leftarrow (0,0)$	3166.195	−0.005	0.959
$(2,2) \leftarrow (1,1)$	3167.890	−0.004	0.966
$(1,3) \leftarrow (0,0)$	3169.919	−0.020	0.666
$(2,0) \leftarrow (1,1)$	3170.429	−0.020	0.196
$(2,4) \leftarrow (1,1)$	3173.702	−0.022	0.467
$(3,2) \leftarrow (3,3)$	3163.378	−0.009	0.993
$(3,1) \leftarrow (2,2)$	3163.707	−0.003	0.989
$(2,1) \leftarrow (2,2)$	3164.281	−0.011	0.992
$(0,2) \leftarrow (1,1)$	3166.340	−0.004	0.871
$(1,2) \leftarrow (1,1)$	3167.392	−0.030	0.942
$(2,3) \leftarrow (2,2)$	3168.343	−0.028	0.860
$(3,3) \leftarrow (2,2)$	3168.737	−0.004	0.891
$(2,1) \leftarrow (2,2)$	3170.931	+0.003	0.298

we have ignored; the fact that we obtain good agreement with experiment without explicitly including these terms in our surface is further evidence that these terms are of minor importance for the dimer bound states considered in this work.

The $S_1(0)$ IR absorption band for $(D_2)_2$ is much richer than that for $(H_2)_2$, and is described in Ref. 26 as "possibly [the] most informative of all the hydrogen dimer spectra" presented there. It contains six pairs of narrow lines separated by the $(D_2)_2$ $v_t=0$ ground-state $J=2 \leftarrow 0$ or $3 \leftarrow 1$ spacings (3.001 and 4.814 cm^{-1}, respectively) and nine additional narrow lines.

The six pairs of lines are associated with transitions from two different rotational levels of the $v_t=0$ ground state to a common $v_t=1$ upper-state level with a firm angular momentum quantum number assignment. The upper part of Table XII compares the computed and experimental transition energies for the higher-frequency transition of each of these pairs. (No additional information about the quality of our potential energy surface is carried by the other transition of each pair.) The agreement between computed and measured transition energies is quite satisfactory; the largest deviation is 0.022 cm^{-1} for the $(J,L)=(2,4) \leftarrow (1,1)$ transition.

In Ref. 25, initial- and final-state quantum number labels were proposed for the nine other narrow lines that appear in the $(D_2)_2$ dimer's $S_1(0)$ IR absorption band; these assignments were described as "less certain" than the assignments for the pairs of lines linked by ground-state combination differences. Eight of these lines are listed in the lower part of Table XII, which shows that using these transition assignments, we again observe very good agreement between computed and measured transition energies. (The one line omitted from Table XII involves a transition to a $J=4$ state whose energy we have not attempted to compute.) Table XII thus confirms the transition assignments proposed in Ref. 25.

TABLE XIII. Observed transition energies and deviations between observed and computed transition energies (computed minus experiment), in cm^{-1}, for IR-active (D$_2$)$_2$ transitions in the D$_2$ $Q_1(0)+S_1(0)$ band. The computed transition energies are obtained using the $(s,q)=(0.0175,0.0235)$ potential energy surface.

$(J,L)' \leftarrow (J,L)''$	Observed	Deviation
$(2,0) \leftarrow (3,3)$	6152.870	−0.018
$(1,1) \leftarrow (2,2)$	6155.672	−0.020
$(2,2) \leftarrow (3,3)$	6155.672	−0.021
$(3,1) \leftarrow (2,2)$	6156.767	−0.015
$(0,2) \leftarrow (1,1)$	6157.770	−0.003
$(1,1) \leftarrow (0,0)$	6158.669	−0.016
$(3,3) \leftarrow (2,2)$	6161.471	−0.036
$(1,2) \leftarrow (1,1)$	6162.773	−0.002
$(2,3) \leftarrow (2,2)$	6163.261	−0.015
$(1,3) \leftarrow (0,0)$	6164.872	−0.005

The upper-state wave functions for the transitions listed in Table XII are linear combinations of radial functions in Eq. (8) with angular momentum quantum numbers $(J,L,j_1,j_2)=(J,L,0,2)$ and $(J,L,2,0)$. For $L \geq 2$, these pairs of radial functions are coupled together by the $A_{2,2,4}$ term of the potential energy surface. In addition, some of the upper states accessed via these transitions are mixtures of $S_1(0)$ states, in which the rotational and vibrational excitation reside on the same D$_2$ monomer, and $Q_1(0)+S_0(0)$ states, in which one monomer is vibrationally excited while the other is rotationally excited; the quantity F listed in Table XII measures the degree of mixing in the upper-state wave functions. The good agreement between computed and observed transition energies in Table XII, especially for transitions to upper states with $L \geq 2$ or with F values below 0.9, indicates that the (r_1,r_2) dependence of our potential energy surface, and of the $A_{2,2,4}$ term in particular, is reasonably accurate.

Further evidence that the (r_1,r_2) dependence of our potential energy surface is accurate comes from Table XIII, where we compare the computed and observed transition energies for several (D$_2$)$_2$ transitions in the dimer's $Q_1(0)+S_1(0)$ overtone IR absorption band. The agreement between computed and observed transition energies is fairly good, although it appears that the potential energy surface generally underestimates slightly the energies of the upper states of these transitions.

VI. PREDICTIONS FOR NOT-YET-OBSERVED TRANSITIONS

In this section, we use our final $(s,q)=(0.0175,0.0235)$ potential energy surface to predict the energies of some not-

TABLE XIV. Predicted transition energies (in cm^{-1}) of the P and R lines in the $Q_1(0)$ IR band of the H$_2$−D$_2$ dimer for vibrationally excited states correlating with $v=0$ H$_2+v=1$ D$_2$. The predictions are obtained using the $(s,q)=(0.0175,0.0235)$ potential energy surface.

$J' \leftarrow J''$	Energy
$1 \leftarrow 2$	2990.889
$0 \leftarrow 1$	2992.044
$1 \leftarrow 0$	2994.732
$2 \leftarrow 1$	2995.909

TABLE XV. Predicted transition energies (in cm^{-1}) for Raman-active transitions in the $Q_1(0)$ band of the (D$_2$)$_2$ dimer. The predictions are obtained using the $(s,q)=(0.0175,0.0235)$ potential energy surface.

$(J,L)' \leftarrow (J,L)''$	Energy
$(1,1) \leftarrow (3,3)$	2988.398
$(0,0) \leftarrow (2,2)$	2990.207
$(0,0) \leftarrow (0,0)$	2993.208
$(1,1) \leftarrow (1,1)$	2993.209
$(2,2) \leftarrow (2,2)$	2993.214
$(3,3) \leftarrow (3,3)$	2993.236
$(2,2) \leftarrow (0,0)$	2996.215
$(3,3) \leftarrow (1,1)$	2998.047

yet-observed IR transitions of the H$_2$−D$_2$ dimer and some not-yet-observed Raman transitions of the (H$_2$)$_2$ and (D$_2$)$_2$ dimers. Experimental studies designed to search for these transitions would help test the accuracy of the potential energy surface presented here.

The region of the H$_2$−D$_2$ dimer's IR absorption spectrum associated with $Q_1(0)$ excitation of the H$_2$ monomer has already been studied experimentally, and as Table X shows, our potential energy surface gives accurate transition energies for the four P and R lines in this portion of the dimer's IR spectrum. The dimer should have four additional IR-active P and R lines associated with $Q_1(0)$ excitation of the D$_2$ monomer. We have computed the transition energies for these four lines based on the dimer binding energies listed in Table VIII; Table XIV lists the predicted transition energies for these four absorption features.

As we noted earlier, the single Raman-active transition in the (H$_2$)$_2$ dimer's $Q_1(0)$ band was recently observed. This dimer should also have Raman-active transitions in the monomer $S_0(0)$ and $S_1(0)$ bands. The energies for these two transitions can be computed from the dimer's ground-state binding energy of 2.895 cm^{-1} and the binding energies of the $(J,L)=(2,0)$ states listed in the second line of Table XI. We therefore predict that the (H$_2$)$_2$ dimer should exhibit $S_0(0)$ and $S_1(0)$ Raman transitions at 354.246 and 4497.415 cm^{-1}, respectively. Unfortunately, these transitions are fairly close to the corresponding Raman-active transitions of the free H$_2$ monomer, which are located at transition energies of 354.373 and 4497.839 cm^{-1}, so a high-resolution experiment will likely be required to observe the dimer transitions.

Because the (D$_2$)$_2$ dimer has four bound states, its Raman spectrum will be much richer than that of (H$_2$)$_2$. In Tables XV and XVI we give predictions for Raman-active transitions of the (D$_2$)$_2$ dimer in the monomer $Q_1(0)$, $S_0(0)$, and $S_1(0)$ bands; these predictions are based on the energy levels listed in Tables IX and XVII. There will be additional Raman features in the dimer's $S_0(0)$ and $S_1(0)$ bands, associated with transitions to final dimer states with $J=3$, which we have omitted from Table XVI because we have not computed the energies of these final dimer states.

VII. SUMMARY AND DISCUSSION

We have presented a six-dimensional H$_2$−H$_2$ potential energy surface that accurately describes several bound (and

TABLE XVI. Predicted transition energies (in cm^{-1}) for Raman-active transitions in the $S_0(0)$ and $S_1(0)$ bands of the $(D_2)_2$ dimer. The predictions are obtained using the $(s,q)=(0.0175,0.0235)$ potential energy surface.

$(J,L)' \leftarrow (J,L)''$	$S_0(0)$ energy	$S_1(0)$ energy
$(0,2) \leftarrow (0,0)$	183.837	3167.595
$(2,0) \leftarrow (0,0)$	178.713	3165.725
$(2,2) \leftarrow (0,0)$	182.694	3168.981
$(1,1) \leftarrow (1,1)$	178.108	3165.208
$(1,3) \leftarrow (1,1)$	184.564	3168.916
$(0,2) \leftarrow (2,2)$	180.836	3164.594
$(2,0) \leftarrow (2,2)$	175.712	3162.724
$(2,2) \leftarrow (2,2)$	179.693	3165.980
$(1,1) \leftarrow (3,3)$	173.298	3160.397
$(1,3) \leftarrow (3,3)$	179.754	3164.105

long-lived quasibound) states of the $(H_2)_2$, $(D_2)_2$, and H_2-D_2 dimers that correlate with H_2 and D_2 monomers in their $(v,j)=(0,0)$, $(0,2)$, $(1,0)$, and $(1,2)$ rovibrational states. The surface is based on a set of *ab initio* H_2-H_2 interaction energies that appear to be nearly converged with respect to the one-electron and many-electron basis sets, and which cover fairly densely the region of configuration space associated with the dimer's van der Waals well. The surface incorporates two empirical adjustments: One softens slightly the surface's repulsive wall at small H_2-H_2 distances, and one increases slightly the magnitude of the surface's $A_{2,2,4}$ term that couples the rotational degrees of freedom of the two monomers. The latter adjustment appears to compensate for the fact that our original $A_{2,2,4}$ coefficients include small contributions from the electrostatic quadrupole-hexadecapole interaction between the two molecules. A FORTRAN subroutine that evaluates the $(s,q)=(0.0175,0.0235)$ potential energy surface is available through EPAPS.[36]

An empirical softening of the *ab initio* H_2-H_2 interac-

TABLE XVII. Energies (in cm^{-1}) for $(D_2)_2$ states with $J_{12}=2$, $v_t=0$ or 1, and $J \leq 2$. The energies are obtained using the $(s,q)=(0.0175,0.0235)$ potential energy surface, and are given relative to the $S_0(0)$ and $S_1(0)$ D_2 monomer energies for $v_t=0$ and 1, respectively.

(J,L)	Exchange symmetry	Energy $v_t=0$	Energy $v_t=1$
(0, 2)	S	−1.942	−5.476
(1, 1)	S	−7.030	−6.881
(1, 2)	S	−5.620	−4.850
(1, 3)	S	−1.238	−3.172
(2, 0)	S	−7.066	−7.347
(2, 1)	S	−5.445	−5.800
(2, 2)	S	−3.085	−4.090
(2, 3)	S	+0.014	−1.754
(0, 2)	A	−6.767	−5.719
(1, 1)	A	−6.654	−6.846
(1, 2)	A	−2.427	−4.692
(1, 3)	A	−0.199	−3.138
(2, 0)	A	−7.172	−7.356
(2, 1)	A	−5.752	−5.821
(2, 2)	A	−4.457	−4.169
(2, 3)	A	−1.813	−1.844

tion energy at small intermolecular distances is not unprecedented. For instance, Schaefer and Kohler[17] found that by softening the short-range repulsive wall of an *ab initio* H_2-H_2 potential energy surface, they could bring properties computed using the surface (in this case, the second virial coefficient of H_2 gas) into better agreement with the experiment. The surface of Diep and Johnson[14] is based on a series of *ab initio* calculations that have been extrapolated to the estimated complete one-electron basis-set limit; this extrapolation technique yields a surface whose repulsive wall is slightly softer than that of the largest basis-set surface explicitly calculated, and thus has the same effect as an empirical softening of the repulsive wall. It would be interesting to compute the H_2-H_2 interaction energy using explicitly correlated electronic structure methods[59] to see whether lingering basis set incompleteness in the present *ab initio* calculations is what necessitates the softening of the short-range repulsive wall of the surface.

We have used our potential energy surface to predict the energies of 34 not-yet-observed IR and Raman transitions for $(H_2)_2$, $(D_2)_2$, and H_2-D_2 dimers involving even-j states of the H_2 and D_2 monomers. Observations of these transitions could help verify the accuracy of the present potential energy surface, or point out areas where the surface could be further improved. Calculations of the energy levels of dimers containing one $j=1$ molecule, such as ortho-H_2–para-H_2, could also be useful in this regard; these calculations are in progress and will be reported in due course.

ACKNOWLEDGMENTS

[1] G. Gallup, Mol. Phys. **33**, 943 (1977).

[2] P. G. Burton and U. E. Senff, J. Chem. Phys. **76**, 6073 (1982).

[3] G. Chałasinski, Mol. Phys. **57**, 427 (1986).

[4] P. Hobza, B. Schneider, J. Sauer, P. Carsky, and R. Zahradnik, Chem. Phys. Lett. **134**, 418 (1987).

[5] H. Lavendy, J. M. Robbe, G. Chambaud, and B. Levy, Chem. Phys. **116**, 11 (1987).

[6] B. Schneider, P. Hobza, and R. Zahradnik, Theor. Chim. Acta **73**, 201 (1988).

[7] U. E. Senff and P. G. Burton, Aust. J. Phys. **42**, 47 (1989).

[8] A. I. Boothroyd, J. E. Dove, W. J. Keogh, P. G. Martin, and M. R. Peterson, J. Chem. Phys. **95**, 4331 (1991).

[9] H. Lavendy, J. M. Robbe, and J. P. Flament, Chem. Phys. Lett. **196**, 377 (1992).

[10] P. Wind and I. Roeggen, Chem. Phys. **167**, 247 (1992).

[11] I. Roeggen and P. Wind, Chem. Phys. **167**, 263 (1992).

[12] P. Wind and I. Roeggen, Chem. Phys. **174**, 345 (1993).

[13] M. Tachikawa, K. Suzuki, K. Iguchi, and T. Miyazaki, Mol. Simul. **12**, 291 (1994).

[14] P. Diep and J. K. Johnson, J. Chem. Phys. **112**, 4465 (2000); **113**, 3480(E) (2000).

[15] C. Kim, S. J. Kim, Y. Lee, and Y. Kim, Bull. Korean Chem. Soc. **21**, 510 (2000).

[16] A. I. Boothroyd, P. G. Martin, W. J. Keogh, and M. R. Peterson, J. Chem. Phys. **116**, 666 (2002).

[17] J. Schaefer and W. E. Köhler, Z. Phys. D: At., Mol. Clusters **13**, 217 (1989).

[18] T. H. Dunning, Jr., J. Chem. Phys. **90**, 1007 (1989).

[19] J. Čižek, J. Chem. Phys. **45**, 4256 (1966).

[20] R. J. Bartlett, J. Phys. Chem. **93**, 1697 (1989).

[21] S. K. Pogrebnya and D. C. Clary, Chem. Phys. Lett. **363**, 523 (2002).

[22] B. Maté, F. Thibault, G. Tejeda, J. M. Fernández, and S. Montero, J. Chem. Phys. **122**, 064313 (2005).

[23] T.-G. Lee, N. Balakrishnan, R. C. Forrey, P. C. Stancil, D. R. Schultz, and G. J. Ferland, J. Chem. Phys. **125**, 114302 (2006).

[24] A. Watanabe and H. L. Welsh, Phys. Rev. Lett. **13**, 810 (1964).

[25] A. R. W. McKellar, J. Chem. Phys. **92**, 3261 (1990).

[26] A. R. W. McKellar, Faraday Discuss. **97**, 69 (1994).

[27] A. R. W. McKellar and J. Schaefer, J. Chem. Phys. **95**, 3081 (1991).

[28] G. Tejeda, J. M. Fernández, S. Montero, D. Blume, and J. P. Toennies, Phys. Rev. Lett. **92**, 223401 (2004).

[29] S. Green, J. Chem. Phys. **62**, 2271 (1975).

[30] M. Abramowitz and I. A. Stegun, *Handbook of Mathematical Functions* (National Bureau of Standards, Washington, DC, 1972).

[31] M. J. Frisch, G. W. Trucks, H. B. Schlegel *et al.*, GAUSSIAN 03, Revision B.03, distributed by Gaussian, Inc., 2003.

[32] K. Raghavachari, G. W. Trucks, J. A. Pople, and M. Head-Gordon, Chem. Phys. Lett. **157**, 479 (1989).

[33] D. E. Woon and T. H. Dunning, Jr., J. Chem. Phys. **100**, 2975 (1994).

[34] S. F. Boys and F. Bernardi, Mol. Phys. **19**, 553 (1970).

[35] F.-M. Tao and Y.-K. Pan, J. Chem. Phys. **97**, 4989 (1992).

[36] See EPAPS Document No. E-JCPSA6-128-006803 for text files containing both the *ab initio* energies and a FORTRAN subroutine that computes the H$_2$−H$_2$ potential energy surface. For more information on EPAPS, see http://www.aip.org/pubservs/epaps.html.

[37] T. Helgaker, H. J. Jensen, P. Joergensen *et al.*, DALTON, Release 1.2.1, a molecular electronic structure program available from http://www.kjemi.uio.no/software/dalton/dalton.html, 2001.

[38] R. J. Hinde, Few-Body Syst. **38**, 187 (2006).

[39] T. van Mourik and T. H. Dunning, Jr., J. Chem. Phys. **111**, 9248 (1999).

[40] R. J. Hinde, J. Phys. B **36**, 3119 (2003).

[41] J. Noga and R. J. Bartlett, J. Chem. Phys. **86**, 7041 (1987).

[42] J. Noga and R. J. Bartlett, J. Chem. Phys. **89**, 3401 (1988).

[43] S. Hirata, J. Phys. Chem. A **107**, 9887 (2003).

[44] E. Aprà, T. L. Windus, T. P. Straatsma *et al.*, NWCHEM, Version 4.7, a computational chemistry package for parallel computers distributed by the U.S. Department of Energy's Pacific Northwest National Laboratory, and available from http://www.emsl.pnl.gov/docs/nwchem/nwchem.html, 2005.

[45] R. A. Kendall, E. Aprà, D. E. Bernholdt, E. J. Bylaska, M. Dupuis, G. I. Fann, R. J. Harrison, J. Ju, J. A. Nichols, J. Nieplocha, Y. P. Straatsma, T. L. Windus, and A. T. Wong, Comput. Phys. Commun. **128**, 260 (2000).

[46] L. Wolniewicz, I. Simbotin, and A. Dalgarno, Astrophys. J., Suppl. Ser. **115**, 293 (1998).

[47] R. J. Hinde, J. Chem. Phys. **122**, 144304 (2005).

[48] A. J. Stone and R. J. A. Tough, Chem. Phys. Lett. **110**, 123 (1984).

[49] T. C. Lillestolen and R. J. Hinde (unpublished).

[50] M. J. Norman, R. O. Watts, and U. Buck, J. Chem. Phys. **81**, 3500 (1984).

[51] J. W. Cooley, Math. Comput. **15**, 363 (1961).

[52] W. Kołos and L. Wolniewicz, J. Chem. Phys. **43**, 2429 (1965).

[53] A. J. Stone and C. P. Woods, Comput. Phys. Commun. **21**, 195 (1980).

[54] R. B. Lehoucq, D. C. Sorensen, and C. Yang, *ARPACK Users' Guide: Solution of Large-Scale Eigenvalue Problems With Implicitly Restarted Arnoldi Methods* (SIAM, Philadelphia, PA, 1998) (ARPACK code is available from http://www.caam.rice.edu/software/ARPACK).

[55] C. C. Paige and M. A. Saunders, SIAM (Soc. Ind. Appl. Math.) J. Numer. Anal. **12**, 617 (1975).

[56] G. Danby, J. Phys. B **22**, 1785 (1989).

[57] J. M. Hutson, BOUND computer code, Version 5, distributed by Collaborative Computational Project 6 of the UK Science and Engineering Research Council, and available from http://www.ccp6.ac.uk/downloads.htm, 1994.

[58] J. E. Grabenstetter and R. J. Le Roy, Chem. Phys. **42**, 41 (1979).

[59] W. Klopper, F. R. Manby, S. Ten-No, and E. F. Valeev, Int. Rev. Phys. Chem. **25**, 427 (2006).